

TRANSPORT AND INSTABILITIES IN MICROCRYSTALLINE SILICON FILMS

S. Reynolds^{*}, V. Smirnov, F. Finger^a, C. Main^b, R. Carius^a

EPICentre, University of Abertay Dundee, Bell Street, Dundee DD1 1HG, U.K.

^aIPV, Forschungszentrum Jülich, 52425 Jülich, Germany

^bUniversity of Dundee, Division of Electronic Engineering and Physics, Nethergate, Dundee DD1 4HN

Coplanar transient photoconductivity and post-transit time-of-flight spectroscopy techniques are used to study carrier transport in microcrystalline silicon films prepared over a range of crystallinities. Although reduced deep defect densities are indicated in more highly crystalline films, this is thought to be an artefact of the shallow Fermi level position. Coplanar samples are susceptible to post-deposition oxidation and reversible adsorption of atmospheric gases, which alter the apparent density of states. A comparison of the results obtained using both techniques suggests that transport is anisotropic, with reduced band tailing (greater structural order) along the direction of film growth, a larger defect concentration around column boundaries, and a higher defect density within the amorphous tissue than in optimised single-component amorphous silicon films.

(Received December 9, 2004; accepted January 26, 2005)

Keywords: Microcrystalline silicon, Transient photoconductivity, Defects, Degradation

1. Introduction

The prospect of further improvements in stable photovoltaic conversion efficiencies provides a strong incentive for research on the optoelectronic properties of microcrystalline silicon ($\mu\text{c-Si:H}$) films [1]. Such films are frequently mixed-phase in character, containing columns or clusters of crystalline grains, disordered regions, voids, and hydrogen [2]. Measurements suggest the presence of band tails and defects, as in hydrogenated amorphous silicon (a-Si:H), but additional complexities are introduced by grain and column boundaries, band offsets and structural anisotropy. However, although carrier transport in this material has been studied intensively for a number of years, there is still no universally-accepted comprehensive electronic model. It has been proposed that dangling bonds are located in the disordered phase around crystalline columns, while boundaries between the smaller grains within columns or larger grains cause deviations in bond lengths and angles, and thus give rise to tail states [3].

For solar cells deposited either by plasma-enhanced chemical vapour deposition (PECVD) [4] or hot-wire (HW) CVD [5], optimal photovoltaic conversion efficiencies are achieved close to the transition to amorphous growth, *i.e.* where the crystalline fraction in the absorber layer is typically 50% [6]. It is believed that in films grown under these conditions loss of minority carriers through recombination at grain boundaries is minimised. However, it has been shown that such films [7], and solar cells [8], may suffer from instabilities due to adsorption of atmospheric components and/or oxidation, and also to some light-induced degradation [5,9].

Transport in disordered materials such as $\mu\text{c-Si:H}$ is strongly influenced by localised states which may act as recombination centres and reduce effective carrier mobilities. A wide range of

* Corresponding author: s.reynolds@abertay.ac.uk

techniques, such as electron spin resonance, the constant photocurrent method and modulated photoconductivity, has been used to probe the defect structure of $\mu\text{c-Si:H}$. In this work, we report transient photoconductivity (TPC) measurements on coplanar films [10], and post-transit time-of-flight (PT-TOF) measurements on solar cells [11], to study the spatial and energetic distribution of defects (density of states, or DOS) as a function of film crystallinity. As TPC and PT-TOF measure currents in orthogonal directions, a comparison of the DOS from each technique might be expected to reveal any isotropic properties [12]. The influence of short- and long-term exposure of coplanar films to room air is also investigated [13], in order to shed light on whether changes in film conductivity are electrostatic in origin or involve a genuine change in the DOS.

2. Experimental details

Samples were prepared at IPV Jülich. Coplanar films were deposited on borosilicate glass in a UHV VHF PECVD system operating at 95 MHz: substrate temperature 185 °C, chamber pressure 0.3 Torr, RF power 5 W [4]. The gas ratio $r = [\text{silane}]/[\text{silane} + \text{hydrogen}]$ was varied between 3.0 and 6.3% to produce a series of films of varying crystallinity. Electrical contacts of length 1 cm and separation 0.05 cm were deposited to form gap cells. Solar cell (p-i-n) structures were deposited in the sequence: glass substrate/TCO/pin/TCO/1 mm² Ag dot contact. The p- and n-layers were prepared using VHF PECVD and the i-layer by HWCVD, with a filament temperature of 1650 °C and a substrate temperature maintained below 220 °C to minimise defect content [5]. For the i-layer, r was varied between 4 and 7%. The ratio of the intensity of the Raman peaks at 480 and 520 cm⁻¹, associated with the amorphous and microcrystalline phases respectively, was used as an indication of film crystallinity; $I_{\text{CRS}} = I_{520}/(I_{480} + I_{520})$.

The transient photocurrent experimental system has been described in detail elsewhere [14]. An electrically-screened Laser Science VSL-337 N₂ laser plus dye attachment was used to generate 4 ns pulses at 640 nm (TPC) and 500 nm (PT-TOF), attenuated as required by neutral density filters. In the TPC work, carrier excitation was typically 10¹⁶ cm⁻³, and the bias voltage was 300 V. In the PT-TOF work the total photogenerated charge was less than the CV-product, a reverse bias of 2 V being used. A specially-designed preamplifier with current offset control was used to nullify the dark current contribution, which could be up to three orders of magnitude greater than the photocurrent at long times. Transients were recorded and averaged on a Tektronix TDS3052 storage oscilloscope, and transferred to a PC for analysis.

Inversion of the current-time data to obtain the DOS was carried out using the Fourier-transform method [15]. In the case of post-transit current analysis, the simple approximate relationship due to Seynhaeve *et al.* [16], $\text{DOS} \propto I \times t$, was found to give similar results.

3. Results and discussion

3.1 Coplanar TPC measurements

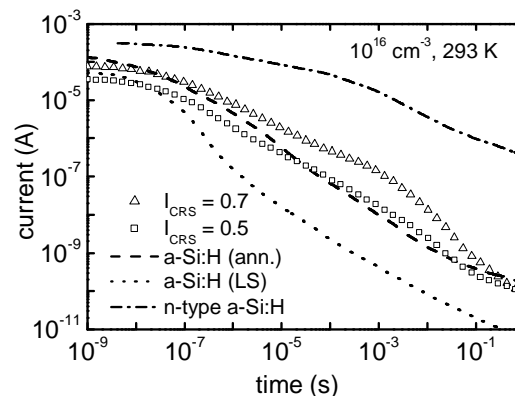


Fig. 1. Current-time decays for $\mu\text{c-Si:H}$ and a-Si:H films.

TPC decays for the coplanar film series are shown in Fig. 1. A trend in the shape of the transients can be identified. For more highly-crystalline films ($I_{CRS} \approx 0.7$), there is a shallow decrease in the photocurrent between 10^{-7} s and 10^{-3} s followed by a more rapid fall extending to the limits of our measurements (1 s). In films approaching the transitional region ($I_{CRS} \approx 0.5$), the initial current is somewhat lower, and tends to follow a featureless power law.

Also shown in Fig. 1 for comparison are TPC decays for light-soaked and annealed intrinsic a-Si:H obtained from an industrial PECVD reactor and for n-type a-Si:H. The n-type sample and the annealed state have conductivity activation energies similar to that of the most crystalline μ c-Si:H sample (0.37 eV) and the transitional μ c-Si:H sample (0.63 eV), respectively. These curves are presented here to enable a comparison between the TPC behaviour of the transitional material and annealed a-Si:H, and the more crystalline material and n-type a-Si:H. This has been explored in more detail in earlier work by the present authors [10] through the intensity- and temperature-dependence of TPC, and also by Brüggemann [17] who used the closely-related modulated photoconductivity technique.

Notwithstanding *bona fide* differences in the DOS between samples, the position of the Fermi level exerts a strong influence on the shape of the TPC decay. The relatively non-dispersive plateau in both n-type amorphous silicon and more crystalline μ c-Si:H is thought to reflect the rôle of minority carrier kinetics in controlling recombination, through charge neutrality considerations [18]. Consequently, the DOS obtained from highly-crystalline samples using ‘spectroscopic’ TPC should be treated with caution, because the linear multiple-trapping model (constant carrier lifetime) on which these methods are predicated is an incomplete description. Furthermore, states deeper than E_F are largely occupied, resulting in an underestimate of the true DOS. The result of applying the spectroscopic analysis to the series of films is shown in Fig. 2(a). The deep defect density appears to decrease with increasing crystallinity, contrary to ESR findings [19].

μ c-Si:H films of composition in the transitional régime behave more consistently when the pulse intensity and experimental temperature are varied, enabling a plausible DOS to be extracted, as shown in Fig. 2(b). This material has a very similar DOS to the commercial a-Si:H film in the annealed state. Other experiments have shown that the transitional material is not as susceptible to light-induced degradation. However, as is also shown in Fig. 3(b), ‘research-grade’ a-Si:H [14] may have a band tail slope of only 20–25 meV, and a substantially lower defect density.

3.2 Effects of exposure to atmosphere

Fig. 3 shows two sets of TPC decays taken on the same sample which was compensated with boron, yielding a low conductivity despite its high crystallinity ($I_{CRS} = 0.8$). One set shows the behaviour some two weeks after deposition (‘as-received’), and the other was taken after six

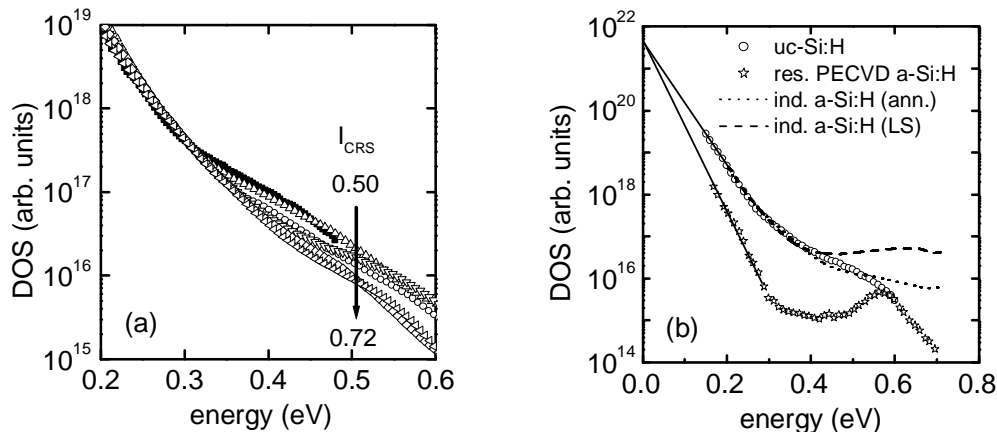


Fig. 2. DOS plots for μ c-Si:H films: (a) vs. crystallinity; (b) in comparison with a-Si:H.

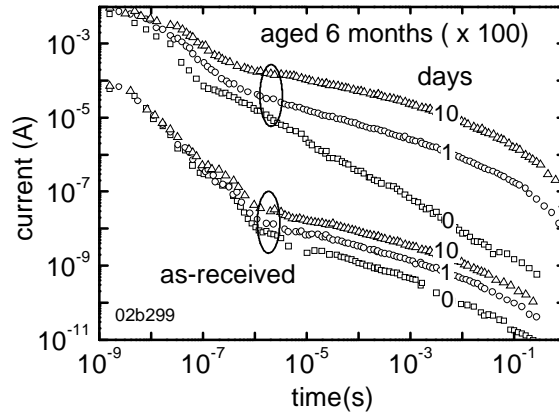


Fig. 3. Effect on TPC decays of exposure to the atmosphere over a period of 6 months.

months' exposure to room air. The procedure followed in each case was that the sample was annealed under vacuum at 160 °C for ten minutes, returned to room temperature, the photocurrent decay recorded without breaking vacuum, and then aged in room air over ten days. Several TPC decays were taken over this period, to track any changes. The general trend observed is similar for both sets of measurements - there is an initial fall in current, steeper than t^{-1} , which reduces in gradient after approximately 1 μ s. The effect of ageing is primarily to reduce the extent of the initial fall, although changes in slope also occur. The rapid fall is associated with deep trapping, and thus the deep defect density is apparently relatively higher in the as-received samples.

Figs. 4(a) and (b) show the corresponding DOS distributions. From TPC measurements at 200 K (not shown here), we were able to determine an ageing-independent conduction band tail slope of approximately 23 meV. Fig. 4(a) reveals a pronounced peak in the DOS for the as-received sample, of the order of 10^{17} cm⁻³ centred at about 0.5 eV. As short-term ageing proceeds, the peak moves to shallower energies. A dark-current activation energy of 0.55 eV in the annealed state indicates that the Fermi level lies close to the centre of the apparent peak in the DOS. Based on the relative changes in the dark current, it moves some 0.15 eV towards the band-edge over the ageing period. This suggests that the reversible effects may be accounted for solely by changes in the space-charge density. A very similar result is seen in a modulated photocurrent experiment, if the electron quasi-Fermi level is moved to shallower energies by increasing the photon flux [14]. Fig. 4(b) shows that after six months, an irreversible reduction of the density of deeper (> 0.45 eV) defects, roughly matched by an increase in the density of shallower defects, has occurred. If this

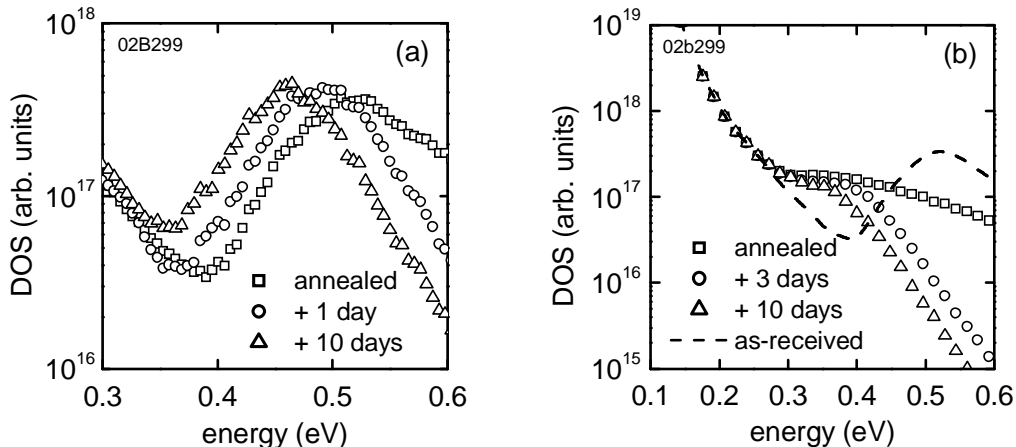


Fig. 4. Effect on DOS of exposure to atmosphere: (a) as-received; (b) six months later.

reflects a true change in the DOS, the electron distribution would re-equilibrate, giving a shift in the Fermi level towards the conduction band edge. This interpretation is supported by a decrease in the dark current activation energy (in the annealed state) from 0.55 eV to 0.48 eV, and an increase in the room temperature dark conductivity by a approximately an order of magnitude over the six-month period. Since it is widely believed that defects in microcrystalline silicon arise at grain boundaries, the long-term change in the DOS may indicate a permanent reconfiguration of dangling bonds, or barrier parameters, due to oxidation. The effects of the ten day ageing cycle are still reversible after six months, and as before may be accounted for by electrostatic effects.

The influence of ageing on the apparent DOS is at least as significant as the spread in crystallinities reported in section 3.1 above. It is therefore no easy task to ascribe portions of the TPC DOS to intrinsic structural features of the film, such as the amorphous tissue or column or grain boundaries, when its properties are so sensitive to post-deposition history. If Figs. 2 and 4 are compared, it can be seen that the effects of varying crystallinity on the DOS are qualitatively similar to those accompanying the ageing process. However, they are not identical. We conclude that the interpretation of structure- or composition-dependent changes in the DOS is made more difficult by uncontrolled atmospheric effects, and accurate comparisons would require measurements to be carried out on films maintained under inert conditions following deposition.

3.3 Post-transit TOF measurements

PT-TOF decays from the sample with $I_{CRS} = 0.32$ are shown in Fig. 5(a), and the resulting DOS in Fig. 5(b). The data have been processed assuming $\nu_0 = 10^{12} \text{ s}^{-1}$, and it is evident there is a good degree of overlap between the DOS sections calculated at different temperatures. This indicates that an appropriate choice has been made for ν_0 , at least for the defect distribution centred at 0.55 eV. At sufficiently low temperatures ($< 200 \text{ K}$) it is possible to observe a section of the conduction band tail. Based on this evidence, the tail slope is quite steep, having a slope of some 18 meV. A crude estimate of the absolute DOS may be made by extrapolating this section to an assumed band edge density of $4 \times 10^{21} \text{ cm}^{-3} \text{ eV}^{-1}$.

Also shown in Fig. 5(b), for comparison, is the DOS obtained for a (slightly thicker) a-Si:H p-i-n device. It can be seen that the DOS is quite similar in shape, though the defect density is lower and the band tail slope slightly larger than for the $\mu\text{c-Si:H}$ device. This suggests that at low crystallinity, the transport process prevailing in both devices is similar, and is consistent with multiple-trapping in tail and defect states.

The effect of temperature on the $I(t)$ decays with increasing i-layer crystallinity is illustrated in Fig. 6(a). There is a tendency for the curves to become temperature-independent for $I_{CRS} > 0.5$, although an increase in gradient is apparent at times longer than 10^{-4} s . However, in

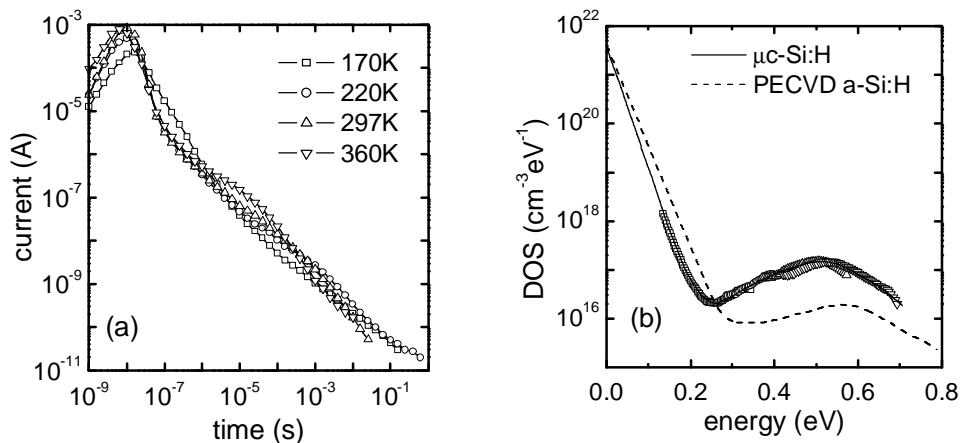


Fig. 5. (a) Current-time; (b) DOS plot for a low-crystallinity film ($I_{CRS} = 0.32$).

more highly crystalline samples the reverse leakage current is several orders of magnitude higher than the photocurrent in this region. Even though the leakage component is nulled out, data below 10^{-10} A should be viewed with caution.

In the context of multiple-trapping theory, it is not possible to construct a realistic DOS that results in a temperature-independent $I(t)$ decay, and so we are obliged to consider what other factors may be influencing transport. On the basis of thermopower measurements, the position of the Fermi level in $\mu\text{-Si:H}$ is believed to move toward the transport level by as much as 0.2 eV between 400 K and 200 K [20]. This could account for the temperature-independent break-point at 10^{-5} s in Fig. 6(a), because although the thermalisation energy sinks more slowly at lower temperatures it may reach the (raised) Fermi level at much the same time. The increased gradient at longer times might also be anticipated, reflecting a sharper thermal distribution of carriers. There is also evidence to suggest that transport below room temperature in highly crystalline films is by hopping [21,22], and the presence of a distribution of states at potential barriers between crystalline clusters or columns and the surrounding amorphous tissue has also been inferred from ESR [23]. If transport does proceed via these pathways, then the shape of the TPC decay is a matter for speculation.

Although the results below room temperature cannot be interpreted consistently in terms of MT theory, this transport mechanism may still prevail at room temperature (and above). If so, comparing the DOS obtained from $I-t$ data at room temperature as the crystallinity is increased, as shown in Fig. 6(b), may give insight into how the defect distributions evolve. As I_{CRS} increases, the peak in the defect distribution moves to shallower energies, suggesting that defects associated with transport in the amorphous material occur in the region of 0.6 eV, and those associated with the presence of the significant microcrystalline component at perhaps 0.4 eV. We pursue this interpretation in the following section.

3.4 Comparison of TPC and PT-TOF results

Fig. 7 is a compilation of several DOS plots presented in previous sections. Data for high-quality amorphous silicon are also included. Each curve is composed of the overlap of DOS segments from measurements made over a range of temperatures, revealing both defect and tail state distributions. The distributions are normalised by extrapolating an assumed exponential band tail to a value of $4 \times 10^{21} \text{ cm}^{-3} \text{ eV}^{-1}$ at the conduction band edge. A comparison suggests that:

- (i) The CB tail slope for $\mu\text{-Si:H}$ deduced for p-i-n structures (albeit rather less crystalline) is considerably steeper than that deduced for coplanar samples.
- (ii) The CB tail slopes for a-Si:H are similar in both coplanar and p-i-n structures - slightly shallower than for $\mu\text{-Si:H}$ p-i-n samples, but somewhat steeper than for coplanar $\mu\text{-Si:H}$.

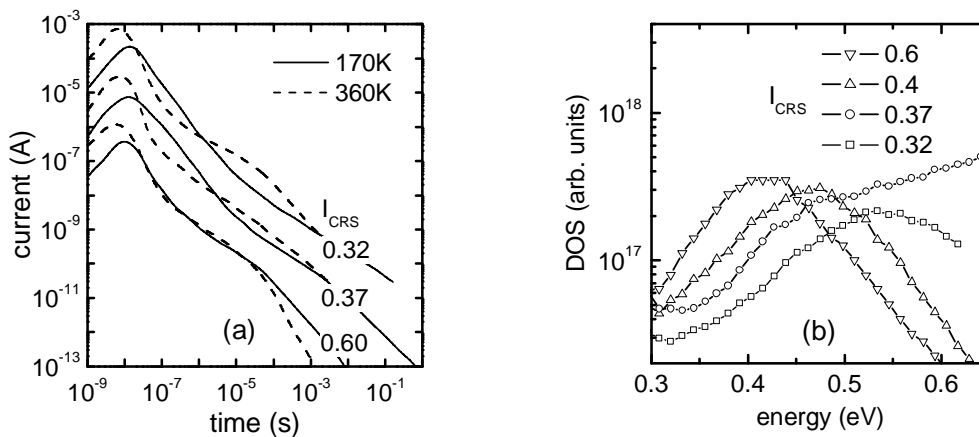


Fig. 6. (a) Effect of increasing film crystallinity on TPC decays (successive curves offset by a factor of 30); (b) DOS calculated from the 300 K curves.

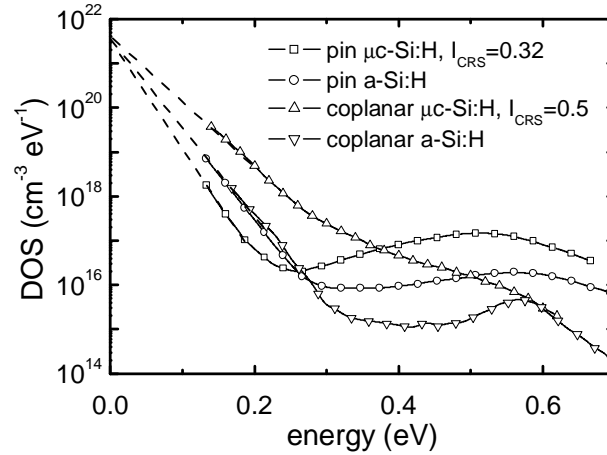


Fig. 7. Comparison of DOS plots obtained from coplanar and p-i-n samples.

- (iii) The deep (>0.6 eV) defect density for coplanar $\mu\text{c-Si:H}$ is lower than that for p-i-n structures.
- (iv) The deep defect density for a-Si:H is lower than for $\mu\text{c-Si:H}$.
- (v) The defect density in coplanar $\mu\text{c-Si:H}$ samples appears to peak in the region of 0.4 eV.

These observations support the view that $\mu\text{c-Si:H}$ films are electrically as well as structurally anisotropic [3,24]. The sharper CB tail sampled by carriers travelling along the direction of growth (PT-TOF on p-i-n samples), rather than in the plane of the film (in TPC on coplanar samples), is consistent with a greater degree of order, as might be found within the crystalline columns. However the higher deep defect density suggests that deep trapping is more prevalent at column boundaries than within the amorphous tissue.

High-quality a-Si:H appears to have a somewhat lower deep defect density than $\mu\text{c-Si:H}$, whichever of the two techniques is used to measure it. This suggests that the amorphous tissue in mixed-phase $\mu\text{c-Si:H}$ is of poorer quality than in single-component a-Si:H. This may be because passivating hydrogen is locked into grain boundaries, and is therefore less readily available to terminate dangling bonds. ESR evidence supports this view: For PECVD material, spin densities as high as 10^{17} cm^{-3} have been reported [19] in highly crystalline samples, falling below 10^{16} cm^{-3} for fully amorphous material. However, in the transitional region between amorphous and microcrystalline growth there is evidence for a minimum in the spin density. At present, we do not possess sufficient photocurrent data on a range of samples (in which atmospheric effects have been excluded) to corroborate this.

4. Conclusions

Coplanar transient photoconductivity and post-transit time-of-flight spectroscopy techniques may be used to probe carrier transport and the density of states in microcrystalline silicon, over a range of crystallinities. Care must be exercised in the interpretation of results from coplanar samples, which are susceptible to post-deposition oxidation and reversible adsorption of atmospheric gases, both of which can alter the apparent density of states. Lower defect densities are suggested for more highly-crystalline films, when measured using coplanar TPC. However, this is, at least in part, an artefact of the up-shifting of the Fermi-level and the consequent increased occupancy of deep states. A more consistent interpretation requires the contribution of minority carrier kinetics to be taken into account. A comparison of results obtained using both techniques on microcrystalline silicon films of similar quality suggests that electronic transport is anisotropic. Measurements are consistent with greater structural order along the direction of film growth, a larger defect concentration around the column boundaries, and a higher defect density within the amorphous tissue than is usual in good-quality 'homogeneous' amorphous silicon films.

Acknowledgments

The authors thank research staff and postgraduate students at IPV Jülich for preparation and characterisation of the samples.

References

- [1] A. V. Shah, J. Meier, E. Vallat-Sauvain, N. Wyrsh, U. Kroll, C. Droz, *Solar Energy Materials & Solar Cells* **78**, 469 (2003).
- [2] L. Houben, M. Luysberg, P. Hapke, R. Carius, F. Finger, H. Wagner, *Philos. Mag. A*, **77**, 1447 (1998).
- [3] J. Kočka, A. Fejfar, H. Stuchlíková, J. Stuchlík, P. Fojtík, T. Mates, B. Rezek, K. Luterová, V. Švrček, I. Pelant, *Solar Energy Materials & Solar Cells* **78**, 493 (2003).
- [4] S. Klein, F. Finger, R. Carius, H. Wagner, M. Stutzmann, *Thin Solid Films* **395**, 305 (2001).
- [5] S. Klein, F. Finger, R. Carius, T. Dylla, B. Rech, M. Grimm, L. Houben, M. Stutzmann, *Thin Solid Films* **430**, 202 (2003).
- [6] O. Vetterl, F. Finger, R. Carius, P. Hapke, L. Houben, O. Kluth, A. Lambertz, A. Mück, B. Rech, H. Wagner, *Solar Energy Materials & Solar Cells* **62**, 97 (2000).
- [7] F. Finger, R. Carius, T. Dylla, S. Klein, S. Okur, M. Günes, *IEE Proc. CDS*, **150**, 300 (2003). (See also this volume.)
- [8] M. Sendova-Vassileva, F. Finger, S. Klein, A. Lambertz, this volume.
- [9] V. Smirnov, S. Reynolds, F. Finger, C. Main, R. Carius, *Mat. Res. Soc. Symp. Proc.* **808**, A9.11 (2004).
- [10] S. Reynolds, V. Smirnov, C. Main, R. Carius, F. Finger, *Mat. Res. Soc. Symp. Proc.* **715**, A21.2.1 (2002).
- [11] S. Reynolds, V. Smirnov, C. Main, R. Carius, F. Finger, *Mat. Res. Soc. Symp. Proc.* **762**, A4.3.1 (2003).
- [12] S. Reynolds, V. Smirnov, C. Main, F. Finger, R. Carius, *Mat. Res. Soc. Symp. Proc.* **808**, A5.7 (2004).
- [13] V. Smirnov, S. Reynolds, C. Main, F. Finger, R. Carius, *J. Non-Cryst. Solids* **338-340**, 421 (2004).
- [14] S. Reynolds, C. Main, D. P. Webb, M.J. Rose, *Phil. Mag. B*, **80**, 547 (2000).
- [15] C. Main, R. Brüggemann, D. P. Webb, S. Reynolds, *Solid St. Commun.* **93**, 401 (1992).
- [16] G. F. Seynhaeve, R. P. Barclay, G. J. Adriaenssens, J. M. Marshall, *Phys. Rev. B*, **39**, 10196 (1989).
- [17] R. Brüggemann, *J. Mater. Sci. – Materials in Electronics* **14**, 629 (2003).
- [18] C. Main, R. Russell, J. Berkin, J. M. Marshall, *Phil. Mag. Lett.* **55**, 189 (1987).
- [19] A. L. Baia Neto, A. Lambertz, R. Carius, F. Finger, *Phys. Stat. Sol. (a)*, **186**, R4-R6 (2001).
- [20] D. Ruff, H. Mell, L. Tóth, I. Sieber, W. Fuhs, *J. Non-Cryst. Solids*, **227-230**, 1011 (1998).
- [21] J. Kočka, H. A. Stuchlíková, J. Stuchlík, B. Rezek, T. Mates, V. Švrček, P. Fojtík, I. Pelant, A. Fejfar, *J. Non-Cryst. Solids* **299-302**, 355 (2002).
- [22] A. Fejfar, N. Beck, H. Stuchlíková, N. Wyrsh, P. Torres, J. Meier, A. Shah, J. Kočka, *J. Non-Cryst. Solids* **227-230**, 1006 (1998).
- [23] F. Finger, J. Müller, C. Malten, H. Wagner, *Philos. Mag. B*, **77**, 805 (1998).
- [24] T. Unold, R. Brüggemann, J. P. Kleider, C. Longeaud, *J. Non-Cryst. Solids* **266-269**, 325 (2000).